3-13-2021

Treatment of diabetic peripheral neuropathy with engineered mesenchymal stromal cell-derived exosomes enriched with microRNA-146a provide amplified therapeutic efficacy

Baoyan Fan
Henry Ford Health, BFAN1@hfhs.org

Michael Chopp
Henry Ford Health, mchopp1@hfhs.org

Zhenggang Zhang
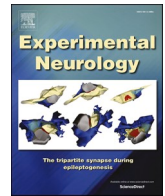*Henry Ford Health*, zzhang1@hfhs.org

Xian Shuang Liu
Henry Ford Health, xliu2@hfhs.org

Follow this and additional works at: https://scholarlycommons.henryford.com/neurology_articles

Recommended Citation

Research paper

Treatment of diabetic peripheral neuropathy with engineered mesenchymal stromal cell-derived exosomes enriched with microRNA-146a provide amplified therapeutic efficacy

Baoyan Fan [a], Michael Chopp [a,b], Zheng Gang Zhang [a], Xian Shuang Liu [a,*]

[a] *Department of Neurology, Henry Ford Health System, Detroit, MI 48202, United States of America*
[b] *Department of Physics, Oakland University, Rochester, MI 48309, United States of America*

A B S T R A C T

Diabetic peripheral neuropathy (DPN) is one of the most prevalent chronic complications of diabetes mellitus with no effective treatment. We recently demonstrated that mesenchymal stromal cell (MSC)-derived exosomes (*exo*-naïve) alleviate neurovascular dysfunction and improve functional recovery. MicroRNA (miRNA), one of the exosomal cargos, downregulates inflammation-related genes, resulting in suppression of pro-inflammatory gene activation. In the present study, we developed engineered MSC-exosomes loaded with miR-146a (*exo*-146a) and compared the therapeutic effects of exo-146a with exo-naïve in diabetic (db/db) mice with DPN. Exo-146a possesses a high loading capacity, robust ability to accumulate in peripheral nerve tissues upon systemic administration, and evokes substantially enhanced therapeutic efficacy on neurological recovery compared with *exo*-naïve. Treatment of DPN in diabetic mice with exo-146a for two weeks significantly increased and decreased nerve conduction velocity, and thermal and mechanical stimuli threshold, respectively, whereas it took four weeks of *exo*-naive treatment to achieve these improvements. Compared with exo-naïve, exo-146a significantly suppressed the peripheral blood inflammatory monocytes and the activation of endothelial cells via inhibiting Toll-like receptor (TLR)-4/NF-κB signaling pathway. These data provide a proof-of-concept about both the feasibility and efficacy of the exosome-based gene therapy for DPN. The translation of this approach to the clinic has the potential to improve the prospects for people who suffer from DPN.

1. Introduction

Diabetic peripheral neuropathy (DPN) is a highly complex and prevalent disease (Pop-Busui et al., 2017). There are currently more than 20 million Americans who have DPN secondary to pre-diabetes, Type I diabetes, or Type II diabetes (Juster-Switlyk and Smith, 2016). The development of DPN closely correlates with neuroinflammation and neurovascular dysfunction in the distal nerves (Hinder et al., 2018; Negi et al., 2011; Zhou and Zhou, 2014). Therapies targeting neuro-inflammation appear to ameliorate nerve dysfunction in experimental DPN (Bierhaus and Nawroth, 2009; Cameron et al., 2005; Hinder et al., 2018; Negi et al., 2010; Sharma et al., 2012; Zhou and Zhou, 2014).

Exosomes are nanovesicles with a diameter ranging from ∼30-100 nm (Thery et al., 2002). They are secreted by most cell types and transported in almost all biological fluids. Exosomes function as natural vehicles of bioactive molecules and thereby mediate intercellular communication (Wang et al., 2020; Zhang et al., 2019). Mesenchymal stromal cell (MSC)-derived exosomes have been reported to suppress the inflammatory immune response and promote the survival and regeneration of injured tissue (Harrell et al., 2019). Our recent study revealed that MSC-derived exosomes alleviate neurovascular dysfunction and facilitate DPN repair primarily by suppression of pro-inflammatory genes (Fan et al., 2020). Bioactive molecule (e.g., mRNA, miRNAs, cytokines, chemokines, immunomodulatory factors) cargos within MSC-

exosomes regulate phenotype, function, and homing of immune cells (Harrell et al., 2019; Phinney et al., 2015). Exosomal miRNAs alter gene expression profiles in their recipient cells, and thereby, influence physiological responses (Kalluri and LeBleu, 2020). MiR-146a is a well-known anti-inflammatory miRNA and is involved in the pathogenesis of DPN (Jia et al., 2016; Wang et al., 2014). Our prior study demonstrated that systemic administration of chemically engineered miR-146a mimics encapsulated within liposomes substantially improves neurovascular function in diabetic mice (Liu et al., 2017). However, liposomes and polymeric nanoparticles have limitations concerning their biocompatibility and long-term safety for clinical use. Moreover, a high dose of oligos produces off-target effects, and the systemic utilization of miRNAs oligo in humans is very expensive and also not applicable for long-term inhibition due to their degradation and rapid dilution. To date, none of the miRNA-based therapies has reached the pharmaceutical breakthrough in clinical trials. The therapeutic miRNAs exhibit low serum stability, off-targeting, and immune responses that hamper their clinical usage (Chakraborty et al., 2017).

Exosome membranes shield their cargos from enzymatic degradation and contain recognition factors that allow them to target recipient cells (Yeo et al., 2013). Emerging reports have shown that exosomes are an efficient vehicle for nucleic acid therapies (Yeo et al., 2013). In contrast to synthetic drug delivery vehicles, the exosome-based delivery system has several advantages, including low immunogenicity, low toxicity, and high nucleic acid loading capacity. Therefore, they hold great promise as vehicles for therapeutic cargo (Escudier et al., 2005).

In the present study, we utilized exosomes released by MSCs as biocompatible nanocarriers for systemic delivery of miR-146a and investigated if engineered MSC-exos enriched with miR-146a augment the therapeutic efficacy of MSC-exos and further improve neurovascular function, as well as the underlying mechanism of action of miR-146a engineered exosomes. These findings provide a rationale for the application of engineered exosomes enriched with miR-146a for the clinical treatment of DPN.

2. Methods

2.1. Construction of engineered MSC-exosome carrying miR-146a (exo-146a)

Mouse bone marrow-derived mesenchymal stromal cells (BM-MSCs, purchased from Thermo Fisher Scientific, Waltham, MA, USA) were transfected with XMIR-146a oligo (SBI System Biosciences, Palo Alto, CA, USA). Briefly, MSCs were seeded in 6-well plate and cultured in D-MEM/F-12 medium containing 5% exosome-depleted FBS (Thermo Fisher Scientific) to 80% confluency. 2 μg XMIR-146a oligo and 7.5 μL lipofectamine 2000 (Thermo Fisher Scientific) were diluted in 250 μL Opti-MEM™ Medium (Thermo Fisher Scientific), respectively before mixture. The DNA-lipid complex was incubated for 15 min at room temperature and added to MSCs for 4 h. The transfection mixture was then removed and added to the exosome-free culture medium. Twenty-four hours post-transfection, the medium was collected, centrifuged at 10,000g for 10 min at 4 °C to remove cellular debris, and used fresh or stored at −80 °C.

To explore the in vivo distribution of MSC-exosomes, we produced GFP-CD63 containing exosomes. Brifely, MSCs were seeded in six-well plates and transfected with 4 μg/well of purified pCMV6-GFP-CD63 (pCMV6-GFP-CD63, OriGene Technologies Inc., Rockville, MD, USA) using lipofectamine 2000 (Thermo Fisher Scientific) for 4 h, then remove the transfection mixture and add to exosome-free culture medium.

The cell culture medium containing exosomes was filtered through 0.22-μm filters. Exosomes were isolated by ultracentrifugation (Beckman Coulter, Brea, CA, USA) at 100,000 g for 2 h at 4 °C (Fan et al., 2020). The exosomes in the pellet were suspended in saline and quantified using Nanosight system (NS300, Cambridge, UK). Western blot

analysis was performed to detect common exosome markers.

2.2. Animals

All animal procedures were approved by the Institutional Animal Care and Use Committee (IACUC) of Henry Ford Hospital and conducted in strict accordance with NIH Guidelines for the Care and Use of Laboratory Animals. Male BKS.Cg-*m*+/+*Leprdb/J* (db/db) mice were purchased from Jackson Laboratories (Bar Harbor, ME, USA). Same aged heterozygote mice (dm) were used as the control. At the age of 20 weeks, db/db mice were randomly divided into the following groups according to a randomization scheme: saline (db/db + vehicle), naïve MSC-exosomes (db/db + *exo*-naïve), and exo-146a (db/db + exo-146a). *N* = 8 per group. Exo-naïve and exo-146a were injected via a tail vein once a week for four consecutive weeks. Db/db group and dm group were administrated with same volume of saline. Glycosylated hemoglobin (HbA1c), glucose (Glc), total cholesterol (TC), and triglyceride (TG) levels in blood were monitored weekly using Accu-check active test strips (Roche Diagnostics, Basel, Switzerland). Serum insulin was tested prior to and after exosome treatment using a mouse ELISA kit (Thermo Fisher Scientific) according to the manufacturer's protocol.

2.3. Mechanical and thermal sensitivity tests

The plantar test was performed to examine the sensitivity of the mice to heat (Fan et al., 2020; Fan et al., 2018). Mice were acclimated for 20 min on a glass surface. A thermal stimulation meter (IITC Life Science, Woodland Hills, CA, USA) was placed under the plantar of the left hind paw. The withdrawal latency in response to the radiant heat (heating intensity was set as 15%) was recorded. Each mouse was tested three times at 15 min intervals. Von Frey test was performed to examine tactile allodynia (Chaplan et al., 1994).

2.4. Neurophysiological measurements

Motor and sensory nerve conduction velocity (MCV, SCV) were examined using orthodromic recording methods (Fan et al., 2020). The electrodes were placed at the right knee and the right sciatic notch of mice under anesthesia. Single square wave current pulses were given by the stimulator (Model 2100, A-M Systems, Sequim, WA, USA). MCV and SCV were calculated according to published studies (Fan et al., 2018; Obrosova et al., 2007).

2.5. Vasa nervorum blood flow

Blood perfusion in plantar and sciatic nerve were measured using laser Doppler perfusion imager (LDPI) system (PeriCam PSI System, Perimed AB, USA) (Fan et al., 2020; Fan et al., 2018). The perfusion color scale was adjusted as 0–250 for plantar and 0–60 for sciatic nerve. The Perfusion Units (PU) in selected regions of interest (ROI) were recorded. Mean perfusion values were calculated within 1 min.

2.6. Myelin sheath staining

The sciatic nerves were processed and cut into 2-μm thick transverse sections as previously described (Fan et al., 2018; Liu et al., 2017). The sections were stained with 1% toluidine blue. The diameter of axons, and myelinated and unmyelinated fibers were measured. The g-ratio was calculated as axon diameter/fiber diameter.

2.7. Immunohistochemistry

Footpad samples were fixed in 4% paraformaldehyde and embedded in paraffin, then cut into sections (6 μm). The primary antibodies used were polyclonal rabbit anti-protein gene product 9.5 (PGP9.5, MilliporeSigma, Burlington, MA, USA) and CD68 (Bio-Rad Laboratories,

Hercules, CA, USA). Normal rabbit IgG (Abcam) was used as a negative control and followed by Cy3-conjugated secondary antibody (Abcam) incubation. The number of PGP 9.5-immunoreactive nerve fiber density was calculated as previously described (Fan et al., 2020; Liu et al., 2017). One section was chosen every ten sections for a total of three cross-sections per animal, which were used for immunostaining.

2.8. Flow cytometry

Blood was collected and monocytes were isolated using Ficoll density gradient centrifugation (MilliporeSigma). The isolated monocytes were suspended in flow cytometry staining buffer (BD Biosciences) and incubated with fluorescence-conjugated antibodies for 30 min at 4 °C. After washing with staining buffer, all samples were resuspended in PBS. Flow cytometry was performed using an SH800 flow cytometer (Sony Biotechnology, San Jose, CA). Antibodies against the following mouse antigens were used: CD11b (PE, 1:100, eBioscience), Ly-6C (APC, 1:100, eBioscience). Three distinct subsets of monocyte were characterized based on Ly-6C expression level: Ly6C$^+$(classical), Ly6C^{int} (intermediate), and Ly6C$^-$(non-classical) monocytes.

2.9. Quantitative real-time RT-PCR (qRT-PCR)

To compare the content of miR-146a in exosomes, *exo*-naïve and exo-146a were lysed in trizol (Qiagen, Valencia, CA, USA). For in vivo miR-146a analysis, sciatic nerve and footpad tissues were dissected from db/db mice treated with exo-naïve or exo-146a ($n = 3$ mice/group) and lysed in trizol. Total RNA in each sample was isolated using miReasy Mini Kit (Qiagen). Reverse transcription was performed using miRNA reverse transcription kit (Applied Biosystem). The program was set as 16 °C 30 min, 42 °C 30 min and 85 °C 5 min. TaqMan® microRNA assays were performed on a ViiA™ 7 real-time PCR Instrument (Applied Biosystem) using TaqMan Universal PCR Master Mix (Applied Biosystem). The program was set as 95 °C 10 min, followed by 95 °C 15 s and 60 °C 1 min for 40 cycles. Each TaqMan assay was done in triplicate for each sample tested. Relative quantities were calculated as the endogenous control using the $2^{-\Delta\Delta Ct}$ method with U6 snRNA as control (4,427,975, ID#000200, Applied Biosystem). Mmu-miR-146a-5p (4,427,975, ID#000468, Applied Biosystem).

2.10. Cell culture

Db/m and db/db mice at the age of 20 weeks were anesthetized and injected intraperitoneally with PBS (containing 5 mmol/l EDTA). Macrophages were elicited and cultured in RPMI-1640 (Gibco, Thermo Fisher Scientific) supplemented with 10% FBS (Gibco) in 24 well plates (10^5 cells/well)(Arroyo et al., 2011). To test the effects of *exo*-naïve and exo-146a on polarization, macrophages were treated with/without exosomes at a concentration of 1×10^6 particles/ml for 48 h. Both cells and medium were collected for further analysis.

To mimic the diabetes-like environment in vitro, human dermal microvascular endothelial cells (HMVECs, ATCC) were cultured with 25 mM glucose for 48 h and then treated with/without exosomes at a concentration of 1×10^6 particles/ml for 48 h. Cells were washed with PBS and lysed with RIPA buffer for Western blot analysis.

Quantification was performed from at least three independent experiments.

2.11. Western blot analysis

Sciatic nerve or footpad dissected from db/db mice treated with/without exosomes were lysed with RIPA buffer containing 1% proteinase and centrifuged at 12,000 g for 15 min at 4 °C to remove debris. Protein concentration in supernatant was measured using BCA assay (Thermo Fisher Scientific). 30 μg of total protein from tissue or HMVEC sample was separated by SDS-PAGE and transferred to PVDF

membranes. After being blocked with 3% BSA blocking buffer, the membranes were incubated with the following antibodies overnight at 4 °C: anti-β-actin (1:2000, Abcam, Cambridge, United Kingdom), inducible nitric oxide synthase (iNOS, 1:1000, EMD Millipore), Arginase-1 (Arg-1, 1:200, Santa Cruz), Toll-like receptor 4 (TLR4, 1:200, Santa Cruz), MyD88 (1:1000, Abcam), NF-KB p65 (1:500, Abcam), interleukin 1 receptor associated kinase 1 (IRAK1, 1:200, Santa Cruz, Dallas, TX, USA), TNF receptor associated factor (TRAF6, 1:200, Santa Cruz), vascular cell adhesion molecule 1 (VCAM-1, 1:500, Abcam), intercellular adhesion molecule 1 (ICAM-1, 1:1000, Abcam), CD9 (1:500, Abcam), CD63 (1:500, Abcam), Alix (1:500, Cell Signaling Technology, Danvers, MA, USA), HSP60 (1:500, Cell Signaling Technology), calreticulin (1:500, Cell Signaling Technology). The next day, the membranes were incubated with secondary antibodies for 2 h and washed. The signals were visualized using an enhanced ECL substrate (Thermo Fisher Scientific). Image J software was used to quantify the band intensity in Western blot images.

2.12. Enzyme-linked immunosorbent assays (ELISA)

ELISA (Thermo Fisher Scientific) was used to quantify TNFα and IL-1β concentrations in the supernatant of cell culture according to the manufacturer's protocol.

2.13. Statistical analysis

Data are presented as mean ± standard deviation (SD). Non-parametric one-way analysis of variance (ANOVA) followed by Tukey's post hoc test was performed for multiple group comparisons. Two-tailed Student's *t*-test was performed for two-group comparisons. A value of $p < 0.05$ was taken as significant.

3. Results

3.1. The therapeutic effect of exo-146a on DPN is superior to exo-naïve

We first characterized exosomes isolated from the supernatant of MSCs transfected with XMIR-146a oligo and found that these exosomes termed as exo-146a had comparable size distribution with naïve MSC-exosomes (*exo*-naïve) assayed by Nanosight analysis (Fig. 1A). Western blot analysis demonstrated that exo-146a contained CD9, CD63, and Alix proteins, but not endoplasmic reticulum markers-calreticulin or HSP60 (Fig. 1B). MiR-146a content within exo-146a was 102.5-fold higher than that in *exo*-naïve (Fig. 1C). These data indicate that *exo*-146a had the general characteristics of exosomes, but carried elevated levels of miR-146a. To examine exosome biodistribution, we first transfected MSCs with pCMV6-AC-GFP plasmid and then isolated the exosomes in the supernatant. We intravenously administered CD63-GFP/exosomes (10^9 particles/mouse) into db/db mice. Twenty-four hours later, the sciatic nerve was collected, fixed, and cut into paraffin sections. As shown in Fig. 1D, CD63-GFP was co-expressed with CD68 (a marker of macrophages) and CD31 (a marker of endothelial cells) suggesting that MSC-exosomes were absorbed by macrophages and endothelial cells, respectively, in peripheral nerve tissues.

To examine the delivery capacity of exosomes in vivo, we administered a one-time injection of *exo*-con and exo-146a (10^9 particles/animal) to db/db mice and collected sciatic nerve tissues 24 h later. The qRT-PCR data indicate that the miR-146a level in the sciatic nerve and footpad tissues were distinctly increased (Fig. 1E) and the expression of miR-146a target genes IRAK1 and TRAF6 were substantially decreased in mice treated with *exo*-146a compared with mice treated with exo-con (Fig. 1F-G).

We recently reported that the treatment of DPN mice with *exo*-naïve for four weeks significantly improved peripheral nerve function (Fan et al., 2020). To examine the effect of exo-146a on DPN, db/db mice were treated with exo-146a or exo-naïve at the dose of 1×10^9 particles/
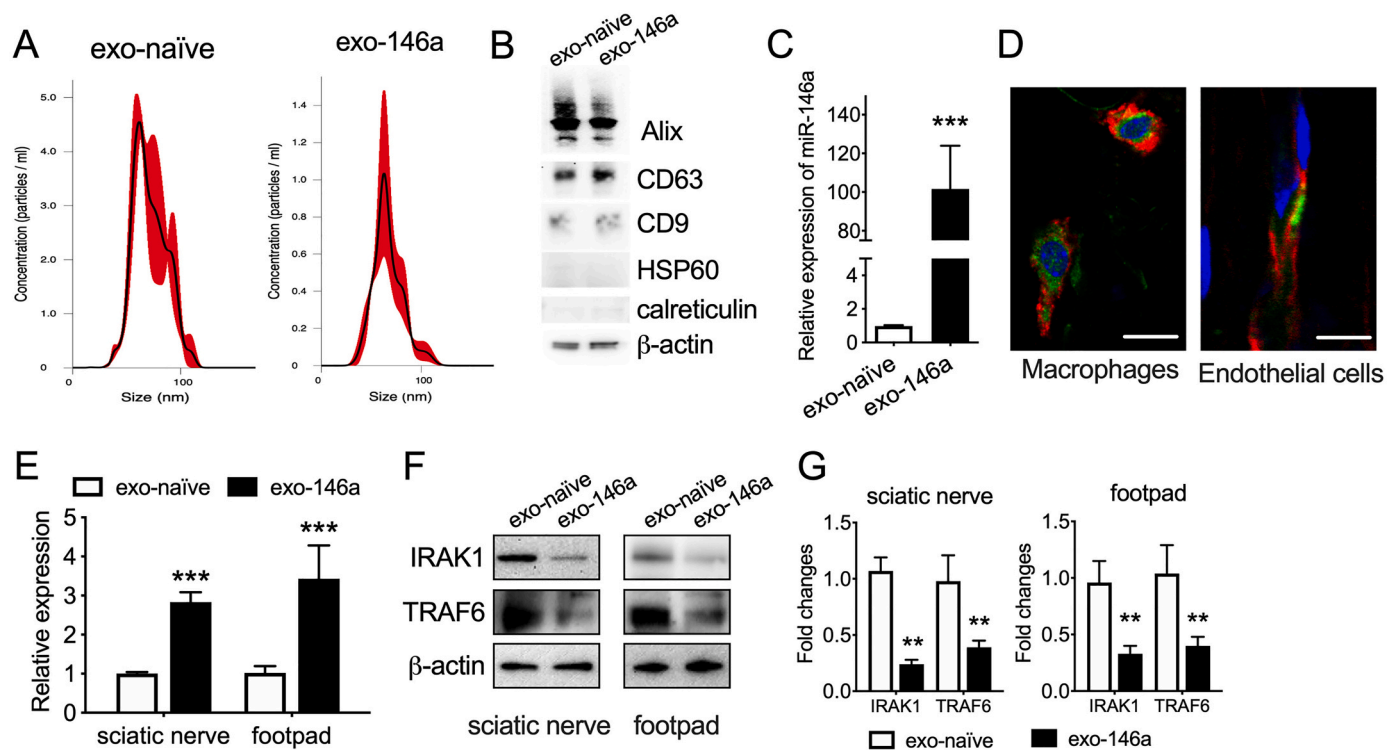
Fig. 1. Engineered MSC-exosomes carry enriched miR-146a. A: Size distribution of *exo*-naïve and exo-146a were measured using the NanoSight system. B: Representative Western blot analysis for exosome markers and endoplasmic reticulum markers in exo-naïve and exo-146a. C: miR-146a expression levels in exo-naïve and exo-146a. D: Representative images of exo-146a (green) internalized by macrophages (CD68^{+}, red) and endothelial cells (CD31^{+}, red) in sciatic nerves. The nuclei were labeled with DAPI (blue), bar = 10 μm. E: Expression of miR-146a in sciatic nerve and plantar tissues. F-G: Representative images and quantification of Western blot analysis for miR-146a target genes IRAK1 and TRAF6 in sciatic nerve and plantar tissues of exo-naïve or exo-146a treated db/db mice. $N = 3$. ** $p <$ 0.01 ***$p < 0.001$ exo-naïve vs exo-146a.

injection once a week for four weeks via tail veins. As expected, compared with non-diabetic mice (dm), db/db mice exhibited DPN, as assayed employing MCV and SCV, plantar, and Von Frey tests before the treatment (Fig. 2A-D). Consistent with our previous finding, db/db mice treated with *exo*-naïve exhibited significant improvement of peripheral neurological function after four weeks of the treatment (Fig. 2A-D)(Fan et al., 2020). However, diabetic mice treated with *exo*-146a for two weeks exhibited significant increases of nerve conduction velocity (Fig. 2A-B), and reduced thermal and mechanical stimuli (Fig. 2C-D). At this time point, *exo*-naïve treated mice did not show obvious changes in nerve conduction or sensitivity. At week-4, both exo-naïve and exo-146a treated db/db mice showed improvement of peripheral neuronal function in the tests, and *exo*-146a treatment induced a more robust and significant effect than did exo-naïve treatment (Fig. 2A-D). These data indicate that the therapeutic effect of exo-146a on DPN is superior to *exo*-naïve. Neither of the exosomes affected the blood levels of glucose or lipid in db/db mice, suggesting the effects of exosomes were not mediated through the alteration of glucose or lipid metabolism (Table. 1).
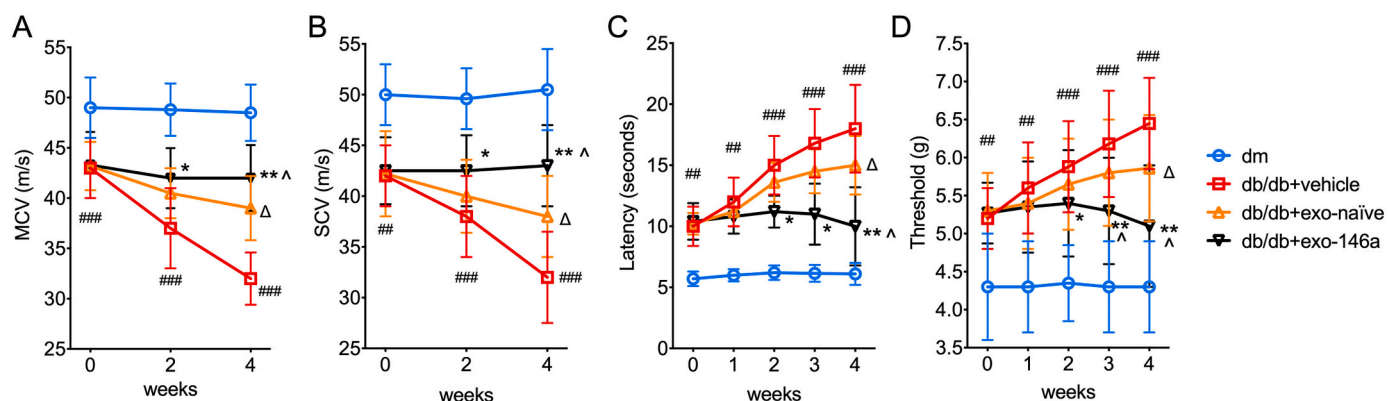

Fig. 2. Exo-146a treatment restores the neurological outcomes db/db mice treated with exo-naïve or exo-146a once per week for 4 weeks. MCV (A) and SCV (B) were tested every two weeks. Threshold to thermal and mechanical stimuli in diabetic mice were by plantar test (C) and Von Frey test (D), respectively. Among the treated groups, exo-146a treated mice showed enhanced neurological outcomes after 2 weeks of administration. ##$p < 0.01$, ###$p < 0.001$ db/db + vehicle vs dm; △$p < 0.05$ db/db + vehicle vs db/db + exo-naïve; *p < 0.05, **p < 0.01 db/db + vehicle vs db/db + exo-146a; ^p < 0.05 db/db + exo-naïve vs db/db + exo-146a. $N =$ 8/group.

Table 1
Concentration of blood glucose, lipids, insulin and body weight.

Feature	Weeks	dm	db/db	db/db + exo-naïve	db/db + exo-146a
Body weight (g)	0	26.2 ± 2.1	42.4 ± 4.4***	44.0 ± 4.2	41.7 ± 6.6
	4	32.5 ± 3.5	48.2 ± 3.5***	50.2 ± 3.6	51.6 ± 4.4
Blood glucose (mmol/l)	0	6.6 ± 0.4	22.1 ± 1.5***	21.9 ± 2.2	22.4 ± 3.2
	4	7.1 ± 1.0	24.4 ± 2.1***	25.8 ± 1.6	27.1 ± 1.6
HbA$_{1c}$ (%)	0	4.0 ± 0.1	9.3 ± 1.6***	9.5 ± 0.8	9.9 ± 1.4
	4	4.1 ± 0.2	10.9 ± 2.1***	10.2 ± 1.2	10.5 ± 1.6
Total cholesterol (mmol/l)	0	2.0 ± 0.3	3.6 ± 0.4***	3.5 ± 0.4	3.7 ± 0.2
	4	2.2 ± 0.1	4.2 ± 0.5***	4.3 ± 0.4	4.3 ± 0.4
Triacylglycerol (mmol/l)	0	0.5 ± 0.1	1.1 ± 0.2**	1.0 ± 0.2	1.1 ± 0.1
	4	0.5 ± 0.1	1.4 ± 0.3***	1.3 ± 0.1	1.4 ± 0.2
Serum Insulin (pmol/l)	0	118.0 ± 15.5	266.0 ± 26.0***	259.0 ± 21.2	267.0 ± 25.5
	4	131.0 ± 17.2	294.0 ± 35.0***	283.0 ± 24.0	291.0 ± 28.8

Values are mean ± SD.** $p < 0.01$, *** $p < 0.001$ db/db vs dm. n = 8/group.

3.2. Exo-146a treatment induces a more robust improvement of neurovascular function in peripheral nerves than treatment with exo-naïve

In peripheral nerves, loss of axons, demyelination, and microvascular dysfunction are related to DPN progression (Cameron et al., 2001; Doupis et al., 2009). Diabetic mice displayed a significant reduction in intraepidermal nerve fiber density (IENFD) in hind paw plantar skin compared with that in dm mice (Fig. 3A-B). Both *exo*-naïve and exo-146a treatments significantly increased IENFD; however, exo-146a treatment showed a more robust augmentation of IENFD (Fig. 3A-B). Exo-naïve and exo-146a significantly restored the diameter of nerve fibers and promoted axon remyelination as well as considerably reduced *g* ratio as compared to the db/db group. In comparison with the same dose of exo-naïve, exo-146a treatment demonstrated a significantly greater impact on the axonal remyelination (Fig. 3C-E). Along with the development of DPN, blood flow perfusion in plantar and sciatic nerves was significantly decreased in the db/db group compared with dm group. Treatment with exo-naïve for four weeks significantly retarded the suppressed blood perfusion flow. Importantly, we found that the treatment of exo-146a further increased regional blood flow by 81% compared with the exo-naïve treated group (Fig. 3F-G).

3.3. Exo-146a treatment induces pronounced immunosuppressive effects

Infiltration of peripheral blood monocytes exacerbates DPN (Sun et al., 2019). Inflammatory monocytes are highly infiltrative and can differentiate into inflammatory macrophages, which cause neurovascular damage (Yang et al., 2014). The peripheral blood collected from db/db mice compared with blood from dm mice contains an elevated level of inflammatory (classical) monocytes, while the administration of *exo*-naïve and exo-146a significantly decrease the percentage of classical monocytes (Fig. 4A-B). Compared with *exo*-naïve, exo-146a treatment exerted a more potent inhibitory inflammatory effect (Fig. 4A-B).

We next investigated the effect of exo-146a treatment on macrophage polarization. Our data demonstrate that db/db mice showed significantly increased activated macrophage accumulation in sciatic nerves, measured by immunohistochemical staining against CD68^{+}. The exo-146a treatment significantly reduced the number of CD68^{+} cells

(Fig. 4C-D). In addition, *exo*-146a treatment significantly inhibits macrophage switching to the M1 phenotype characterized by iNOS and enhances the formation of the M2-like phenotype characterized by Arg-1 (Fig. 4G-H). Moreover, treatment with exo-146a suppresses the secretion of pro-inflammatory cytokines TNFα and IL-1β (Fig. 4E-F). We previously reported MSC-exos containing miRNAs synergistically downregulate the TLR4/NF-κB signaling pathway (Fan et al., 2020). Data from the present study reveal that miR-146a within exosomes inhibited its target gene IRAK1 and enhance the inhibition of TLR4, MyD88, and NF-κB expression. These data provide insight into why the effects of *exo*-146a on macrophages are more pronounced than those of exo-naïve (Fig. 4G-H).

3.4. Exo-146a treatment amplifies the impact of exo-naïve on the attenuation of diabetes-induced endothelial dysfunction

Hyperglycemia-induced activation of ECs increases inflammatory mediators, which enhance endothelial interactions with leukocytes and the sensitization of primary afferent neurons (De Caterina et al., 2000). We, therefore, examined whether exo-146a treatment modulates diabetes-induced activation of sciatic nerve endothelial cells. The expression of VCAM-1 and ICAM-1 were significantly increased in the sciatic nerves of db/db mice compared with dm mice. Exo-146a treatment significantly reduced the levels of these proteins, while exo-naïve did not provide a pronounced effect on these adhesion molecules (Fig. 5A-B).

Next, we examined whether exo-146a alters the inflammatory activation of HMVECs cultured in HG medium. Western blot analysis demonstrated that exo-146a showed a robust inhibitory effect on ICAM-1 and VCAM-1 expression (Fig. 5C-D). Both sets of exosomes inhibited HG-induced expression of TLR4, NF-κB, and TNFα, and exo-146a significantly reduced expression of these inflammatory mediators compared with exo-naïve (Fig. 5C-D). These findings highlight the protective roles of exo-146a on endothelial function and may at least partially explain its therapeutic effects on reducing neurovascular damage.

4. Discussion

In the present study, we employed engineered MSC-exosomes carrying enriched miR-146a (*exo*-146a) to treat db/db mice with DPN. In comparison to the treatment with exosomes isolated from naïve MSCs (exo-naïve), treatment with exo-146a amplifies and enhances the anti-inflammatory and protective effects on neurological function and promotes neurorecovery in mice with DPN. Our data provide not only new insights into the molecular mechanisms of MSC-exosome therapy but also a proof-of-principle for MSC-exosomes to deliver a specific miRNA as cargo to the peripheral nervous system.

Engineered exosomes are proposed as a biological nanoplatform for clinical drug delivery (van den Boorn et al., 2013). Compared with synthetic nanoscale particles, exosomes showed increased delivery and therapeutic efficacy because of their biocompatibility and the capacity to escape degradation (Luan et al., 2017; van der Meel et al., 2014; Zhang et al., 2019). Exosomes have natural targeting ability based on donor cells, and their size range allows them to easily penetrate deep tissue (Luan et al., 2017; Zhang et al., 2019). These favorable features drive efforts to engineer exosomes for the targeted delivery of exogenous nucleic acids and therapeutic drugs to target tissues (Mendt et al., 2018). MSC-derived exosomes have emerged as an attractive and safe experimental application in the treatment of stroke, neural injury, neurodegenerative diseases, and cancer (Phinney and Pittenger, 2017; Xin et al., 2013a; Xiong et al., 2017; Zhang et al., 2019).

One of the widely used approaches for loading therapeutic genes into exosomes involves transfecting parent cells to overexpress the gene. Our group engineered miR-enriched MSC-exosomes for the treatment of stroke and observed that the miR cargo robustly enhanced the
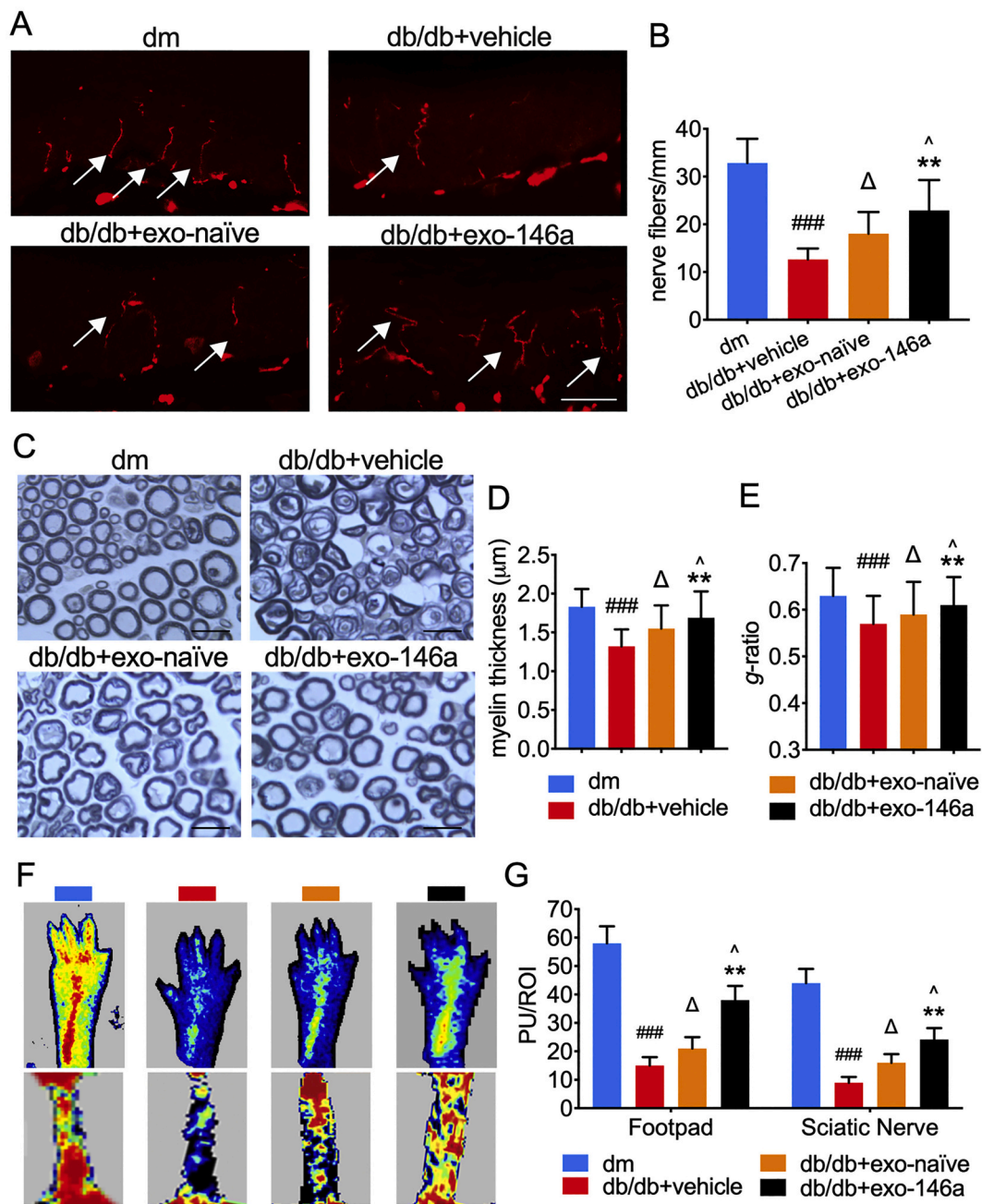
Fig. 3. Exo-146a treatment improves neurovascular perfusion and prevents the impairment in the peripheral nervous system. A-B: Representative immunofluorescent images and quantification of PGP9.5 staining IENF in hind paw plantar skin of all groups. Bar = 50 μm. C: Semi-thin toluidine blue tained cross sections of sciatic nerves. Bar = 20 μm. D-E: Quantification of myelin thickness and g-ratio in sciatic nerve. F: Laser Doppler images of the planter and sciatic nerve of mice. Flux within tissues was measured and perfusion signal was expressed as different colors. Blood flow from low to high are marked as dark blue-green-yellow-red. G: Quantification of blood flow measurement results are expressed in Perfusion Units (PU)/ Regions of Interest (ROI). $^{###}p < 0.001$ db/db + vehicle vs dm; $^{\Delta}p < 0.05$ db/db + vehicle vs db/db + exo-naïve; $^{**}p < 0.01$ db/db + vehicle vs db/db + exo-146a; $^{\wedge}p < 0.05$ db/db + exo-naïve vs db/db + exo-146a. N = 8/group.

therapeutic effect of naïve exosomes (Xin et al., 2017; Xin et al., 2013b; Zhang et al., 2017). These findings confirmed that engineered exosomes for miRNA delivery is feasible, practical and avoids the high cost and the potential adverse effects of using miRNA mimic the in vivo treatment. We previously reported that *exo*-naïve reduce the inflammatory response and thereby improved the neurological outcomes in db/db mice with DPN (Fan et al., 2020). To amplify their anti-inflammatory activity, we loaded miR-146a oligo into MSCs and produced miR-146a enriched exosomes. The transfection did not affect the basic properties of exosomes including marker expression and particle secretion. We showed that exo-146a is transferred to peripheral nerves and induces a

relatively high level of miR-146a in target tissues. Our data also demonstrated the therapeutic effects of exo-146a are at least in part mediated via the regulation of diabetic chronic inflammation by regulating miR-146 target genes, which indicates that the enriched miR-146a increases the immunomodulatory effects of naïve MSC-exosomes in DPN. Compared with exo-naïve, exo-146a shorten the therapy duration and achieved better recovery outcomes, indicating that the therapeutic effects of exo-146a are superior to those of *exo*-naïve. These findings add to the growing body of evidence that exosome-delivered miRNAs are part of the cell-cell communication network that coordinates immune responses. Although we do not exclude the possibility that the
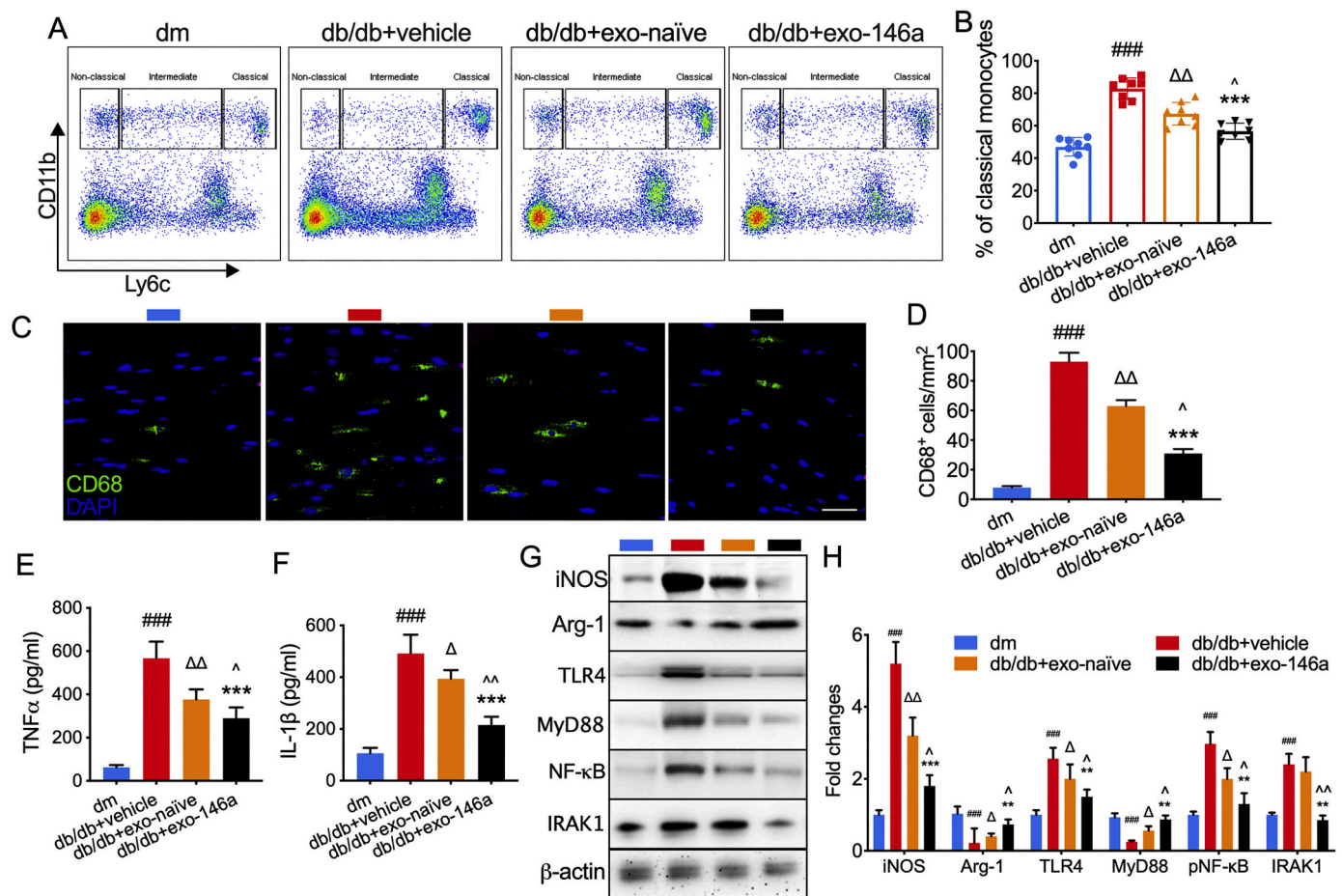
Fig. 4. Effects of exo-146a treatment on inflammatory response. A–B: Monocyte subsets in the blood were characterized by CD11b and Ly6C staining. A: Representative pattern plot of monocyte subsets in the peripheral blood of mice. B: Quantification of monocyte subsets. N = 8/group. C–D: Representative immunofluorescent images and quantitative data of active macrophages (CD68$^+$ cells) in sciatic nerve. E–F: Exo-naïve and exo-146a inhibited the secretion of TNFα and IL-1β in the supernatant from intraperitoneal macrophages cultures tested using ELISA. G–H: Representative images of Western blot analysis and the relative expression levels of iNOS, Arg-1, TLR4, MyD88, and NF-κB in macrophages. N = 3/group. ###$p < 0.001$ db/db + vehicle vs dm; $^\Delta p < 0.05$, $^{\Delta\Delta} p < 0.01$ db/db + vehicle vs db/db + exo-naïve; **$p < 0.01$, ***$p < 0.001$ db/db + vehicle vs db/db + exo-146a; ^$p < 0.05$, ^^$p < 0.01$ db/db + exo-naïve vs db/db + exo-146a.

transfection may have an impact on the exosome cargo, the observed therapeutic effect of exo-146a confirms the potential of MSC-exosomes as a miRNA vehicle for the treatment of DPN. Additional studies for the development the high scale and efficient production of clinical-grade exosomes are warranted.

We and others previously reported the anti-inflammatory role of MSC-exosomes in a mouse model of DPN (Fan et al., 2020; Phinney et al., 2015; Zhang et al., 2014). Wiklander et al. reported that most of the injected MSC-derived extracellular vesicles accumulated in the mononuclear phagocyte system (Wiklander et al., 2015). The unbalanced monocyte phenotype in peripheral blood has an adverse impact on foot ulcer healing in diabetes patients (Mirza and Koh, 2011). In the present study, loading MSC-exosomes with miR-146a significantly augmented the effects of exo-naïve on the differentiation pattern of monocytes in peripheral blood. Furthermore, exo-146a provided more potent effects on the alteration of macrophage polarization and suppressed the secretion of TNFα and IL-1β via inhibiting the TLR4/NF-κB pathway than exo-naïve. These data indicate that exo-146a inhibits inflammation by suppressing macrophage infiltration and M1 macrophage polarization in sciatic nerves, and decreases the production of cytokines that can activate the vascular endothelium and alter the sensory transduction properties of axons, which in concert ameliorates DPN. It is noteworthy that the majority of exo-146a were detected in macrophages and endothelial cells of sciatic nerves. This may provide insight into the robust reduction of inflammation mediated by exo-146a.

Further studies on the cell-specific internalization of MSC-exosomes are warrented.

Chronic inflammation induces disruption of insulin signaling, leading to vascular complications in diabetes (Reddy et al., 2012; Shoelson et al., 2006). The anti-inflammatory miR-146a exerts protective effects on ECs in a mouse model of diabetic nephropathy (Bhatt et al., 2016; Huang et al., 2014). However, to our knowledge there have been no reports about the association of miR-146a with endothelial cell function in the progression of DPN. Our data demonstrate that exo-146a treatment significantly reduces diabetes-induced expression of ICAM-1 and VCAM-1, while exo-naïve treatment did not show an obvious difference from control. Exo-146a reduces the synthesis of inflammatory cytokines by inhibiting the TLR4/NF-kB pathway, which at least partially explains the protective effects of exo-146a on peripheral nerve axons in db/db mice. Further studies are needed to investigate the effects of exo-146a on micro/macro vessel repair and the interaction of the affected vasculature with leukocytes that may contribute to the reduction of blood vessel dysfunction in peripheral nerves resulting from exo-146a treatment of DPN.

5. Conclusion

In summary, our data demonstrate that exosomes as biologic vehicles of miR-146a can effectively mediate and enhance the therapeutic activity of MSCs in diabetic mice, providing a novel therapeutic strategy
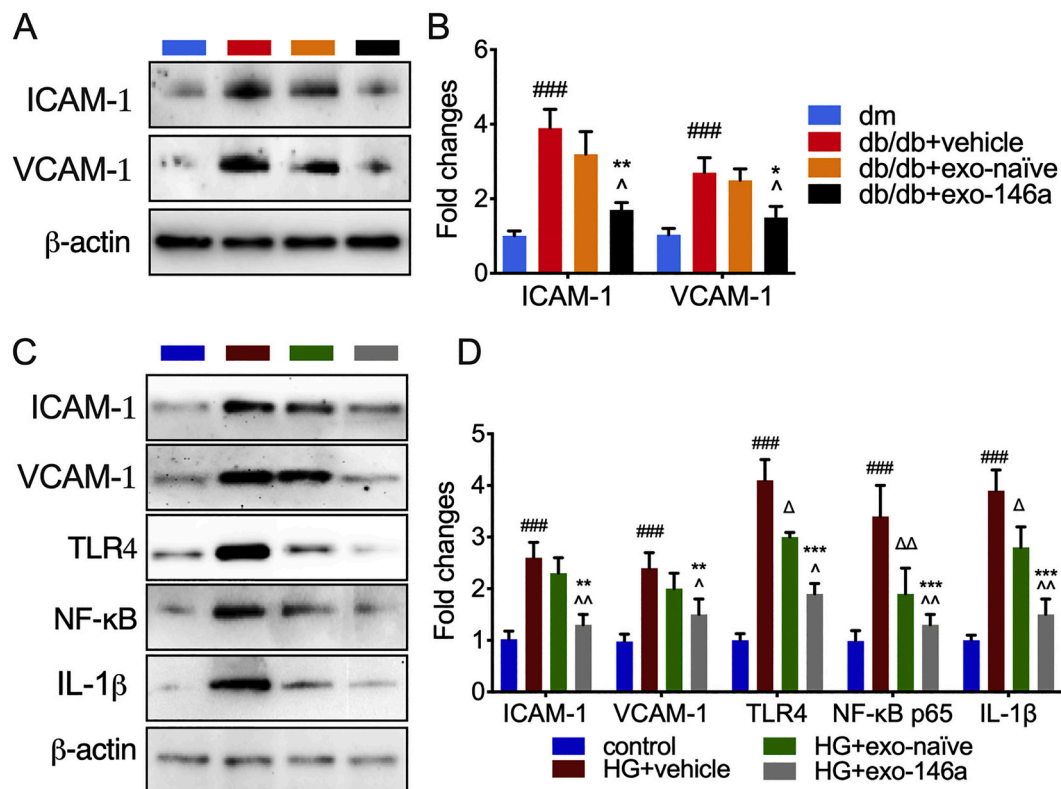
Fig. 5. Exo-146a treatment attenuates diabetes-induced activation of endothelial cells. A-B: Representative images of Western blot analysis and the relative expression levels of ICAM-1 and VCAM-1 in sciatic nerves of db/db mice with DPN. N = 3/group. [###]$p < 0.001$ db/db + vehicle vs dm; [Δ]$p < 0.05$ db/db + vehicle vs db/db + exo-naïve; *$p < 0.05$ **$p < 0.01$ db/db + vehicle vs db/db + exo-146a; ^$p < 0.05$ db/db + exo-naïve vs db/db + exo-146a. C-D: Representative images of western blot analysis and the relative expression levels of ICAM-1, VCAM-1, TLR4, NF-κB and TNFα in HMVECs. N = 3/group. [###]$p < 0.001$ HG + vehicle vs control; [Δ]$p < 0.05$, [ΔΔ]$p < 0.01$ HG + vehicle vs HG + exo-naïve; **$p < 0.01$, ***$p < 0.001$ HG + vehicle vs HG + exo-146a; ^$p < 0.05$, ^^$p < 0.01$ HG + exo-naïve vs HG + exo-146a.

for the benefit of neurovascular remodeling and functional recovery of DPN. This approach also provides a new platform that can be applied to other miRNAs that regulate the development of DPN. Although promising data are emerging, the possibility that MSC-exosomes may be employed in clinical use depends on the scaling of exosome production and the quality, reproducibility, and potency of the exosomes, which will require much effort. However, there is reason to believe that this cutting-edge technology will have great therapeutic potential for patients with DPN.

Declaration of Competing Interest

There are no conflicts of interest that relate to our manuscript.

Acknowledgments

Appendix A. Supplementary data

Supplementary data to this article can be found online at https://doi. org/10.1016/j.expneurol.2021.113694.

References

Arroyo, J.D., Chevillet, J.R., Kroh, E.M., Ruf, I.K., Pritchard, C.C., Gibson, D.F., Mitchell, P.S., Bennett, C.F., Pogosova-Agadjanyan, E.L., Stirewalt, D.L., Tait, J.F., Tewari, M., 2011. Argonaute2 complexes carry a population of circulating microRNAs independent of vesicles in human plasma. Proc. Natl. Acad. Sci. U. S. A. 108, 5003–5008.

Bhatt, K., Lanting, L.L., Jia, Y., Yadav, S., Reddy, M.A., Magilnick, N., Boldin, M., Natarajan, R., 2016. Anti-inflammatory role of MicroRNA-146a in the pathogenesis of diabetic nephropathy. J. Am. Soc. Nephrol. 27, 2277–2288.

Bierhaus, A., Nawroth, P.P., 2009. Multiple levels of regulation determine the role of the receptor for AGE (RAGE) as common soil in inflammation, immune responses and diabetes mellitus and its complications. Diabetologia 52, 2251–2263.

Cameron, N.E., Eaton, S.E., Cotter, M.A., Tesfaye, S., 2001. Vascular factors and metabolic interactions in the pathogenesis of diabetic neuropathy. Diabetologia 44, 1973–1988.

Cameron, N.E., Gibson, T.M., Nangle, M.R., Cotter, M.A., 2005. Inhibitors of advanced glycation end product formation and neurovascular dysfunction in experimental diabetes. Ann. N. Y. Acad. Sci. 1043, 784–792.

Chakraborty, C., Sharma, A.R., Sharma, G., Doss, C.G.P., Lee, S.S., 2017. Therapeutic miRNA and siRNA: moving from bench to clinic as next generation medicine. Mol. Ther. Nucleic Acids 8, 132–143.

Chaplan, S.R., Bach, F.W., Pogrel, J.W., Chung, J.M., Yaksh, T.L., 1994. Quantitative assessment of tactile allodynia in the rat paw. J. Neurosci. Methods 53, 55–63.

De Caterina, R., Liao, J.K., Libby, P., 2000. Fatty acid modulation of endothelial activation. Am. J. Clin. Nutr. 71, 213S–223S.

Doupis, J., Lyons, T.E., Wu, S., Gnardellis, C., Dinh, T., Veves, A., 2009. Microvascular reactivity and inflammatory cytokines in painful and painless peripheral diabetic neuropathy. J. Clin. Endocrinol. Metab. 94, 2157–2163.

Escudier, B., Dorval, T., Chaput, N., Andre, F., Caby, M.P., Novault, S., Flament, C., Leboulaire, C., Borg, C., Amigorena, S., Boccaccio, C., Bonnerot, C., Dhellin, O., Movassagh, M., Piperno, S., Robert, C., Serra, V., Valente, N., Le Pecq, J.B., Spatz, A., Lantz, O., Tursz, T., Angevin, E., Zitvogel, L., 2005. Vaccination of metastatic melanoma patients with autologous dendritic cell (DC) derived-exosomes: results of thefirst phase I clinical trial. J. Transl. Med. 3, 10.

Fan, B., Liu, X.S., Szalad, A., Wang, L., Zhang, R., Chopp, M., Zhang, Z.G., 2018. Influence of sex on cognition and peripheral neurovascular function in diabetic mice. Front. Neurosci. 12, 795.

Fan, B., Li, C., Szalad, A., Wang, L., Pan, W., Zhang, R., Chopp, M., Zhang, Z.G., Liu, X.S., 2020. Mesenchymal stromal cell-derived exosomes ameliorate peripheral neuropathy in a mouse model of diabetes. Diabetologia 63, 431–443.

Harrell, C.R., Jovicic, N., Djonov, V., Arsenijevic, N., Volarevic, V., 2019. Mesenchymal stem cell-derived exosomes and other extracellular vesicles as new remedies in the therapy of inflammatory diseases. Cells 8.

Hinder, L.M., Murdock, B.J., Park, M., Bender, D.E., O'Brien, P.D., Rumora, A.E., Hur, J., Feldman, E.L., 2018. Transcriptional networks of progressive diabetic peripheral neuropathy in the db/db mouse model of type 2 diabetes: an inflammatory story. Exp. Neurol. 305, 33–43.

Huang, Y., Liu, Y., Li, L., Su, B., Yang, L., Fan, W., Yin, Q., Chen, L., Cui, T., Zhang, J., Lu, Y., Cheng, J., Fu, P., Liu, F., 2014. Involvement of inflammation-related miR-155 and miR-146a in diabetic nephropathy: implications for glomerular endothelial injury. BMC Nephrol. 15, 142.

Jia, L., Wang, L., Chopp, M., Zhang, Y., Szalad, A., Zhang, Z.G., 2016. MicroRNA 146a locally mediates distal axonal growth of dorsal root ganglia neurons under high glucose and sildenafil conditions. Neuroscience 329, 43–53.

Juster-Switlyk, K., Smith, A.G., 2016. Updates in diabetic peripheral neuropathy. F1000Res 5.

Kalluri, R., LeBleu, V.S., 2020. The biology, function, and biomedical applications of exosomes. Science 367.

Liu, X.S., Fan, B., Szalad, A., Jia, L., Wang, L., Wang, X., Pan, W., Zhang, L., Zhang, R., Hu, J., Zhang, X.M., Chopp, M., Zhang, Z.G., 2017. MicroRNA-146a mimics reduce the peripheral neuropathy in type 2 diabetic mice. Diabetes 66, 3111–3121.

Luan, X., Sansanaphongpricha, K., Myers, I., Chen, H., Yuan, H., Sun, D., 2017. Engineering exosomes as refined biological nanoplatforms for drug delivery. Acta Pharmacol. Sin. 38, 754–763.

Mendt, M., Kamerkar, S., Sugimoto, H., McAndrews, K.M., Wu, C.C., Gagea, M., Yang, S., Blanko, E.V.R., Peng, Q., Ma, X., Marszalek, J.R., Maitra, A., Yee, C., Rezvani, K., Shpall, E., LeBleu, V.S., Kalluri, R., 2018. Generation and testing of clinical-grade exosomes for pancreatic cancer. JCI Insight 3.

Mirza, R., Koh, T.J., 2011. Dysregulation of monocyte/macrophage phenotype in wounds of diabetic mice. Cytokine 56, 256–264.

Negi, G., Kumar, A., Kaundal, R.K., Gulati, A., Sharma, S.S., 2010. Functional and biochemical evidence indicating beneficial effect of Melatonin and Nicotinamide alone and in combination in experimental diabetic neuropathy. Neuropharmacology 58, 585–592.

Negi, G., Kumar, A., Sharma, S.S., 2011. Melatonin modulates neuroinflammation and oxidative stress in experimental diabetic neuropathy: effects on NF-kappaB and Nrf2 cascades. J. Pineal Res. 50, 124–131.

Obrosova, I.G., Ilnytska, O., Lyzogubov, V.V., Pavlov, I.A., Mashtalir, N., Nadler, J.L., Drel, V.R., 2007. High-fat diet induced neuropathy of pre-diabetes and obesity: effects of "healthy" diet and aldose reductase inhibition. Diabetes 56, 2598–2608.

Phinney, D.G., Pittenger, M.F., 2017. Concise review: MSC-derived exosomes for cell-free therapy. Stem Cells 35, 851–858.

Phinney, D.G., Di Giuseppe, M., Njah, J., Sala, E., Shiva, S., St Croix, C.M., Stolz, D.B., Watkins, S.C., Di, Y.P., Leikauf, G.D., Kolls, J., Riches, D.W., Deiuliis, G., Kaminski, N., Boregowda, S.V., McKenna, D.H., Ortiz, L.A., 2015. Mesenchymal stem cells use extracellular vesicles to outsource mitophagy and shuttle microRNAs. Nat. Commun. 6, 8472.

Pop-Busui, R., Boulton, A.J., Feldman, E.L., Bril, V., Freeman, R., Malik, R.A., Sosenko, J. M., Ziegler, D., 2017. Diabetic neuropathy: a position statement by the American Diabetes Association. Diabetes Care 40, 136–154.

Reddy, M.A., Jin, W., Villeneuve, L., Wang, M., Lanting, L., Todorov, I., Kato, M., Natarajan, R., 2012. Pro-inflammatory role of microrna-200 in vascular smooth muscle cells from diabetic mice. Arterioscler. Thromb. Vasc. Biol. 32, 721–729.

Sharma, A., Bernatchez, P.N., de Haan, J.B., 2012. Targeting endothelial dysfunction in vascular complications associated with diabetes. Int. J. Vasc. Med. 2012, 750126.

Shoelson, S.E., Lee, J., Goldfine, A.B., 2006. Inflammation and insulin resistance. J. Clin. Invest. 116, 1793–1801.

Sun, J.J., Tang, L., Zhao, X.P., Xu, J.M., Xiao, Y., Li, H., 2019. Infiltration of blood-derived macrophages contributes to the development of diabetic neuropathy. J Immunol Res 2019, 7597382.

Thery, C., Zitvogel, L., Amigorena, S., 2002. Exosomes: composition, biogenesis and function. Nat. Rev. Immunol. 2, 569–579.

van den Boorn, J.G., Dassler, J., Coch, C., Schlee, M., Hartmann, G., 2013. Exosomes as nucleic acid nanocarriers. Adv. Drug Deliv. Rev. 65, 331–335.

van der Meel, R., Fens, M.H., Vader, P., van Solinge, W.W., Eniola-Adefeso, O., Schiffelers, R.M., 2014. Extracellular vesicles as drug delivery systems: lessons from the liposome field. J. Control. Release 195, 72–85.

Wang, L., Chopp, M., Szalad, A., Zhang, Y., Wang, X., Zhang, R.L., Liu, X.S., Jia, L., Zhang, Z.G., 2014. The role of miR-146a in dorsal root ganglia neurons of experimental diabetic peripheral neuropathy. Neuroscience 259, 155–163.

Wang, L., Chopp, M., Szalad, A., Lu, X., Zhang, Y., Wang, X., Cepparulo, P., Lu, M., Li, C., Zhang, Z.G., 2020. Exosomes derived from Schwann cells ameliorate peripheral neuropathy in type II diabetic mice. Diabetes 69, 749–759.

Wiklander, O.P., Nordin, J.Z., O'Loughlin, A., Gustafsson, Y., Corso, G., Mager, I., Vader, P., Lee, Y., Sork, H., Seow, Y., Heldring, N., Alvarez-Erviti, L., Smith, C.I., Le Blanc, K., Macchiarini, P., Jungebluth, P., Wood, M.J., Andaloussi, S.E., 2015. Extracellular vesicle in vivo biodistribution is determined by cell source, route of administration and targeting. J. Extracell Vesicles 4, 26316.

Xin, H., Li, Y., Cui, Y., Yang, J.J., Zhang, Z.G., Chopp, M., 2013a. Systemic administration of exosomes released from mesenchymal stromal cells promote functional recovery and neurovascular plasticity after stroke in rats. J. Cereb. Blood Flow Metab. 33, 1711–1715.

Xin, H., Li, Y., Liu, Z., Wang, X., Shang, X., Cui, Y., Zhang, Z.G., Chopp, M., 2013b. MiR-133b promotes neural plasticity and functional recovery after treatment of stroke with multipotent mesenchymal stromal cells in rats via transfer of exosome-enriched extracellular particles. Stem Cells 31, 2737–2746.

Xin, H., Katakowski, M., Wang, F., Qian, J.Y., Liu, X.S., Ali, M.M., Buller, B., Zhang, Z.G., Chopp, M., 2017. MicroRNA cluster miR-17-92 cluster in exosomes enhance neuroplasticity and functional recovery after stroke in rats. Stroke 48, 747–753.

Xiong, Y., Mahmood, A., Chopp, M., 2017. Emerging potential of exosomes for treatment of traumatic brain injury. Neural Regen. Res. 12, 19–22.

Yang, J., Zhang, L., Yu, C., Yang, X.F., Wang, H., 2014. Monocyte and macrophage differentiation: circulation inflammatory monocyte as biomarker for inflammatory diseases. Biomark. Res. 2, 1.

Yeo, R.W., Lai, R.C., Zhang, B., Tan, S.S., Yin, Y., Teh, B.J., Lim, S.K., 2013. Mesenchymal stem cell: an efficient mass producer of exosomes for drug delivery. Adv. Drug Deliv. Rev. 65, 336–341.

Zhang, B., Yin, Y., Lai, R.C., Tan, S.S., Choo, A.B., Lim, S.K., 2014. Mesenchymal stem cells secrete immunologically active exosomes. Stem Cells Dev. 23, 1233–1244.

Zhang, Y., Chopp, M., Liu, X.S., Katakowski, M., Wang, X., Tian, X., Wu, D., Zhang, Z.G., 2017. Exosomes derived from mesenchymal stromal cells promote axonal growth of cortical neurons. Mol. Neurobiol. 54, 2659–2673.

Zhang, Z.G., Buller, B., Chopp, M., 2019. Exosomes - beyond stem cells for restorative therapy in stroke and neurological injury. Nat. Rev. Neurol. 15, 193–203.

Zhou, J., Zhou, S., 2014. Inflammation: therapeutic targets for diabetic neuropathy. Mol. Neurobiol. 49, 536–546.